
EXAM PROJECT FOR PML 2022/2023

REPORT

Christian Dybdahl Troelsen
Department of Computer Science
University of Copenhagen
Universitetsparken 1
DK-2100 Copenhagen Ø
tfp233@alumni.ku.dk

Jens Sørensen
Department of Computer Science
University of Copenhagen
Universitetsparken 1
DK-2100 Copenhagen Ø
qrw992@alumni.ku.dk

Mathias Rasmussen
Department of Computer Science
University of Copenhagen
Universitetsparken 1
DK-2100 Copenhagen Ø
tjc725@alumni.ku.dk

January 18, 2023

1 Density modeling

1.1 Implement a convolutional VAE

Architecture of the convolutional VAE Our implementation of the convolutional VAE (CVAE) is similar in architecture to the original VAE. The primary difference between the two models is that the two linear layers in the encoder and decoder part of the original VAE have been replaced by respectively two convolutional layers and two transposed convolutional layers in the convolutional VAE. The two convolutional layers in the encoder part of the CVAE both use kernels of size 3×3 , 1×1 padding and a stride of 2×2 . The first convolutional layer has 1 input channel and 16 output channels, while the second convolutional layers has 16 input channels and 32 output channels. The transposed convolutional layers in the decoder part of the CVAE complement the aforementioned convolutional layers. Both transposed convolutional layers use kernels of size 3×3 , 1×1 padding 1×1 , output padding and a stride of 2×2 . The first transposed convolutional layer has 32 input channels and 16 output channels, while the second transposed convolutional layers has 16 input channels and 1 output channel. Conceptually, the encoder part of the CVAE condenses its input images \mathbf{x} of size $D = N \times N$ into a compact but feature rich representation \mathbf{z} of size $C = 2$, while the corresponding decoder "unfolds" this compact representation in reverse order, ultimately producing output images \mathbf{y} of the same size as \mathbf{x} .

Parameter estimation In order to optimize the CVAE model we estimate the parameters ϕ and θ that maximize the ELBO, which is a lower bound on the log likelihood of the data \mathbf{x} and is defined as $\mathcal{L}(\theta, \phi, \mathbf{x}) = \mathbb{E}_{q_\phi(\mathbf{z}|\mathbf{x})}[\ln p_\theta(\mathbf{x}|\mathbf{z})] - \text{KL}(q_\phi(\mathbf{z}|\mathbf{x})||p_\theta(\mathbf{z}))$. This is the same criterion used to optimize the original VAE. In particular, both models use the reparameterization trick to sample latent variables \mathbf{z} from a factorized gaussian approximate posterior $q_\phi(\mathbf{z}|\mathbf{x}) = \mathcal{N}(\mathbf{z}; \boldsymbol{\mu}, \text{diag}(\boldsymbol{\sigma}^2))$, so the Kullback-Leibler divergence, which acts as a regularization term in the ELBO, simplifies to $\frac{1}{2} \sum_{d=1}^D (\sigma_d^2 + \mu_d^2 - 1 - \ln(\sigma_d^2))$, assuming that the prior over \mathbf{z} is also a diagonal gaussian $p_\theta(\mathbf{z}) = \mathcal{N}(\mathbf{z}; \mathbf{0}, \mathbf{I})$. Here $\ln \boldsymbol{\sigma}^2$ and $\boldsymbol{\mu}$ are the outputs of the encoder when applied to \mathbf{x} . In order to compute the first term in the ELBO, which is the expected likelihood of \mathbf{x} given \mathbf{z} , we utilize the output \mathbf{y} of the decoder. We fed \mathbf{y} fed through a sigmoid activation layer, which produces the mean parameters \mathbf{p} of a factorized multivariate Bernoulli distribution $\prod_j^D \text{Bernoulli}(x_j; p_j)$ acting as the likelihood $p_\theta(\mathbf{x}|\mathbf{z})$ of the input \mathbf{x} given latent variable \mathbf{z} . We then approximate the expected log likelihood by computing the negative of the binary cross entropy of \mathbf{p} and \mathbf{x} , where \mathbf{x} is treated as a set of probability values. Given the simplified ELBO, we optimize the parameters of both models using a variant of gradient descent, namely the Adam algorithm with a learning rate of 0.001 and a batch size of 128. In order to ensure convergence we run the Adam algorithm for a total of 25 epochs for each model. We train both models on the complete MNIST training set.

Performance of VAE models We compare the performance of the two VAE models on the MNIST test set using two quantitative measures and three qualitative experiments. The two quantitative measures are the sample-wise

mean ELBO on the MNIST test set and the MSE loss between samples from the MNIST test set and corresponding reconstructions produced by the VAE models. The three qualitative experiments are

1. Clustering MNIST test data in latent space by mapping each observation \mathbf{x}_i to corresponding mean parameters $\boldsymbol{\mu}_i$ using the encoder and subsequently plotting these $\boldsymbol{\mu}_i$ with colors based on the actual labels t_i associated with each \mathbf{x}_i .
2. Exploring the latent space by sampling latent variables \mathbf{z} deterministically from a regular grid, then using the decoder to map these \mathbf{z} to corresponding mean parameters \mathbf{p} , and finally visualizing these \mathbf{p} as images.
3. Reconstructing selected observations \mathbf{x}_i from the MNIST test set by mapping these to posterior distributions $q_\phi(\mathbf{z}_i|\mathbf{x}_i)$, then randomly sampling \mathbf{z}_i from these posterior distributions, and finally using the decoder to map these \mathbf{z}_i to corresponding mean parameters \mathbf{p}_i , which are finally interpreted as reconstruction of the inputs \mathbf{x}_i .

A comparison of the sample-wise ELBO and MSE loss for the two VAE models is shown in Table 1. As can be seen, both models seem to have a sample-wise mean ELBO that is on the same scale as well as an MSE loss that is on the same scale. However, it is also apparent that both the sample-wise mean ELBO and the MSE loss is slightly better for the original VAE than for the CVAE. This indicates that the VAE has learned a slightly better approximation of the density implicitly defined by the MNIST test set as well as being slightly better at reconstructing images from the MNIST test set. The clustering of the MNIST test data shown in Figure 3a and Figure 3b indicate a similar relationship between the performance of the two models. In particular, we see that both models seem to have learned a representation in latent space that is capable of separating most samples from the MNIST test set based on class labels. That being said, it also clear that the CVAE struggles more than the VAE with separating some samples based on class labels, in particular those representing digits 4, 7, and 9.

The exploration of latent space shown in Figure 2a and Figure 2b corroborate the idea that the VAE is better at separating classes. Note in particular how the mean parameter images produced by the VAE seem to be slightly more well-defined (i.e. less blurry) than those produced by the CVAE. It is also worth noting that the exploration of latent space in the CVAE seem to produce a greater variety of digits than does the corresponding exploration of latent space in the VAE (it seems to mainly produce 6s, 0s, 2s, 1s and 9s). The reconstruction results shown in Figure 1b and Figure 1c also indicate that the VAE is somewhat superior to the CVAE, in this case in terms of accurately reconstructing samples from the MNIST test set. This is most obvious when considering the reconstructions of digits 2 and 4, which the VAE has rendered reasonably clearly, contrary to the CVAE, which has rendered them somewhat blurry. In particular, it seems that the CVAE has trouble distinguishing 4 from 9.

The reason why the CVAE slightly underperforms compared to the VAE is not entirely clear to us. In fact, one might expect the CVAE would perform better than the VAE, given that convolutional layers in general are better than linear layers at capturing complex spatial information in image data. One reason why the CVAE underperforms may be that the MNIST dataset is too simple and hence convolutional layers are not required to extract its most salient features. In particular, since MNIST digits are centered and of similar size, the convolutional layers might not be necessary. Its also possible that the CVAE is not deep enough to effectively learn a useful representation of the MNIST data, that the kernel size (3×3) used by its layers is not large enough to capture spatial dependencies in the MNIST data or that a stride of (2×2) results in too significant a loss of information.

1.2 Alternative models

1.2.1 Probabilistic PCA

Essential properties and advantages/disadvantages The first model which we implement is the probabilistic PCA model introduced in Chapter 12.2.1 of [Bishop and Nasrabadi, 2006]. The reason this model is attractive is primarily due to the fact that its likelihood is tractable. In particular, given a dataset $\mathbf{X} = \{\mathbf{x}_n\}$ of N samples \mathbf{x}_n with D dimensions each, the log likelihood of the PPCA model is given by $\ln p(\mathbf{X}|\mathbf{W}, \mathbf{u}, \sigma^2) = -\frac{N}{2} (D \ln(2\pi) + \ln |\mathbf{C}| + \text{Tr}(\mathbf{C}^{-1}\mathbf{S}))$, where $\mathbf{C} = \mathbf{W}\mathbf{W}^T + \sigma^2\mathbf{I}$ and \mathbf{S} is the sample covariance matrix of \mathbf{X} . Moreover, there exists a closed form-solution for the parameters \mathbf{W} , \mathbf{u} , σ^2 , which maximize this log-likelihood.

The existence of a closed-form expression for the likelihood function is useful, as it allows for direct comparison with other density model. The fact that its the maximizing parameters also have a closed-form means we can easily optimize the PPCA model. At the same time, the PPCA model also allows for numerical optimization using the Expectation-Maximization (EM) algorithm, which can be more efficient in higher dimensions and when dealing with missing data. From a practical point of view, the PPCA model is useful, as it can be used both for dimensionality-reduction (like the regular PCA model), but also for random sampling due to its probabilistic nature. Finally, a major advantage of the PPCA model is that it allows capturing the most important covariance in its included principal components, while averaging the variance for all the remaining left-out principal components in its parameter σ^2 .

Perhaps the most obvious disadvantage of the PPCA model is that it is based on a linear-gaussian framework and hence, unlike the VAE, may not be able to capture complex non-linear structure in the data it is trained on. On another note, it is worth pointing out that the maximum-likelihood solution to the PPCA model only determines the latent space up to an arbitrary rotation \mathbf{R} . We shall for simplicity set $\mathbf{R} = \mathbf{I}$. Moreover, we shall use $M = 2$ principal components, so that we may easily compare the latent space of the PPCA model with that of the previously introduced VAE models.

Model performance We assess whether the PPCA model is better or worse than the original VAE by using the same quantitative measures and quality experiments used to compare the CVAE with the VAE in the previous section. For the MSE loss we compare images \mathbf{x}_i from the MNIST test set with corresponding mean parameter values $\boldsymbol{\eta}_i$ obtained by first mapping each \mathbf{x}_i to a posterior distribution $p(\mathbf{z}_i|\mathbf{x}_i) = \mathcal{N}(\mathbf{z}|\text{proj}(\mathbf{x}_i), \sigma^2 \mathbf{M}^{-1})$, where $\text{proj}(\mathbf{x}_i) = \mathbf{M}^{-1} \mathbf{W}^T (\mathbf{x}_i - \boldsymbol{\mu})$ and $\mathbf{M} = \mathbf{W}^T \mathbf{W} + \sigma^2 \mathbf{I}$, then sampling a \mathbf{z}_i from this distribution, and finally computing $\boldsymbol{\eta}(\mathbf{x}_i) = \mathbf{W} \mathbf{z}_i + \boldsymbol{\mu}_i$. This same procedure is used for the reconstruction experiment, though in this case we compare select \mathbf{x}_i and corresponding $\boldsymbol{\eta}_i$ visually. For the clustering experiment, we reuse the projection $\text{proj}(\mathbf{x}_i)$ to map each sample \mathbf{x}_i to its corresponding mean parameter in latent space. Symmetrically, for the exploration of latent space we reuse the back-projection $\boldsymbol{\eta}(\mathbf{x}_i)$ for mapping the deterministically sampled latent variables \mathbf{z}_i to corresponding mean parameters that are subsequently represented as images.

1.2.2 Gaussian Mixture Model

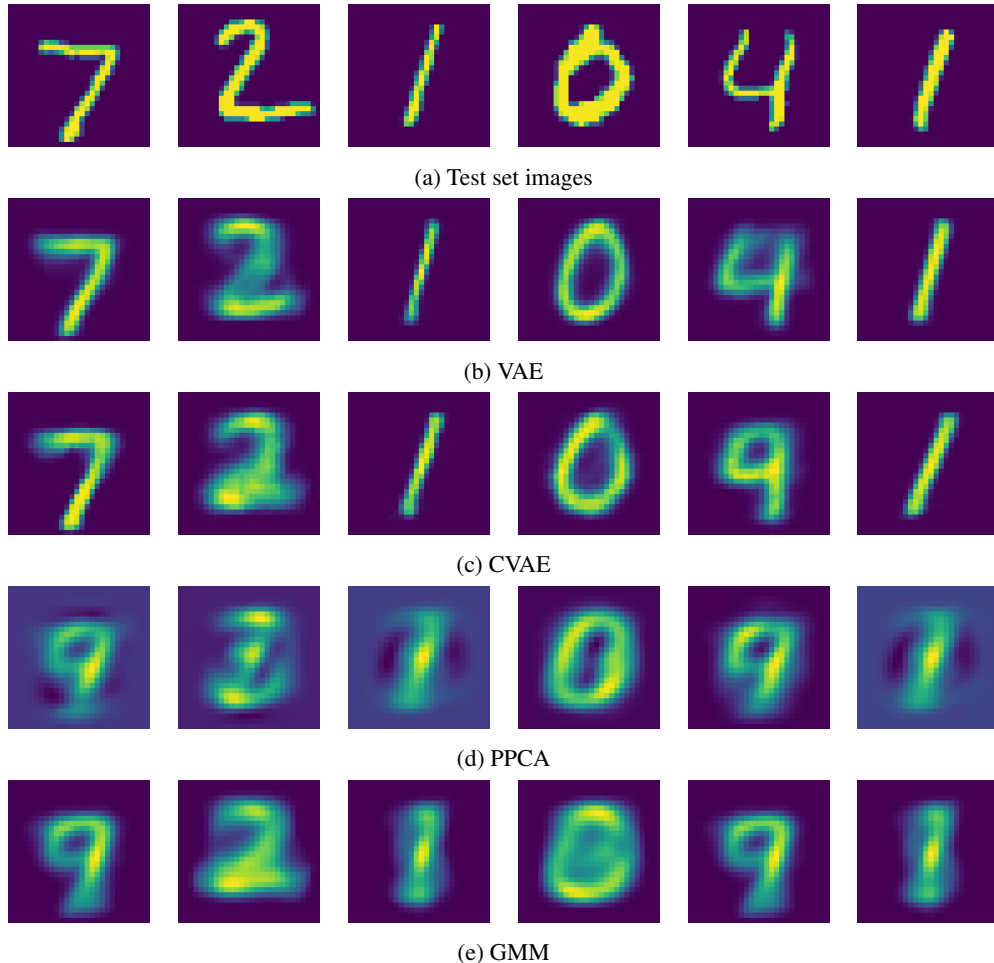


Figure 1: Comparison of MNIST test set images and corresponding mean parameters generated by density models

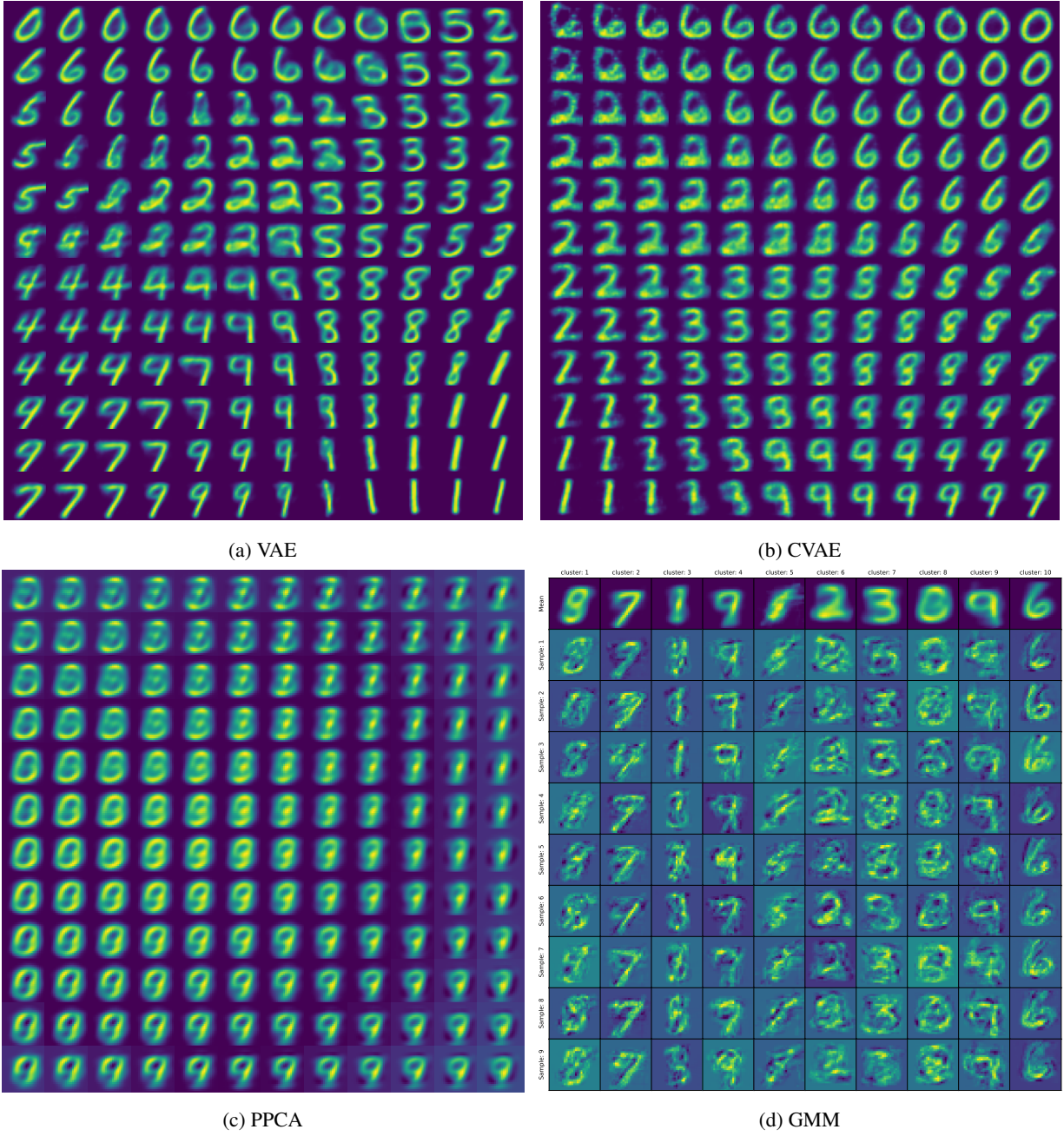


Figure 2: Interpolating images from latent space variables using trained density models.

	Log-Likelihood/ELBO	MSE
VAE	-1.428134e+02	0.037524
CVAE	-1.568176e+02	0.044254
PPCA	-4.329656e+03	3629.250732
GMM	-1.067011e+07	3831.718461

Table 1: Model performance metrics

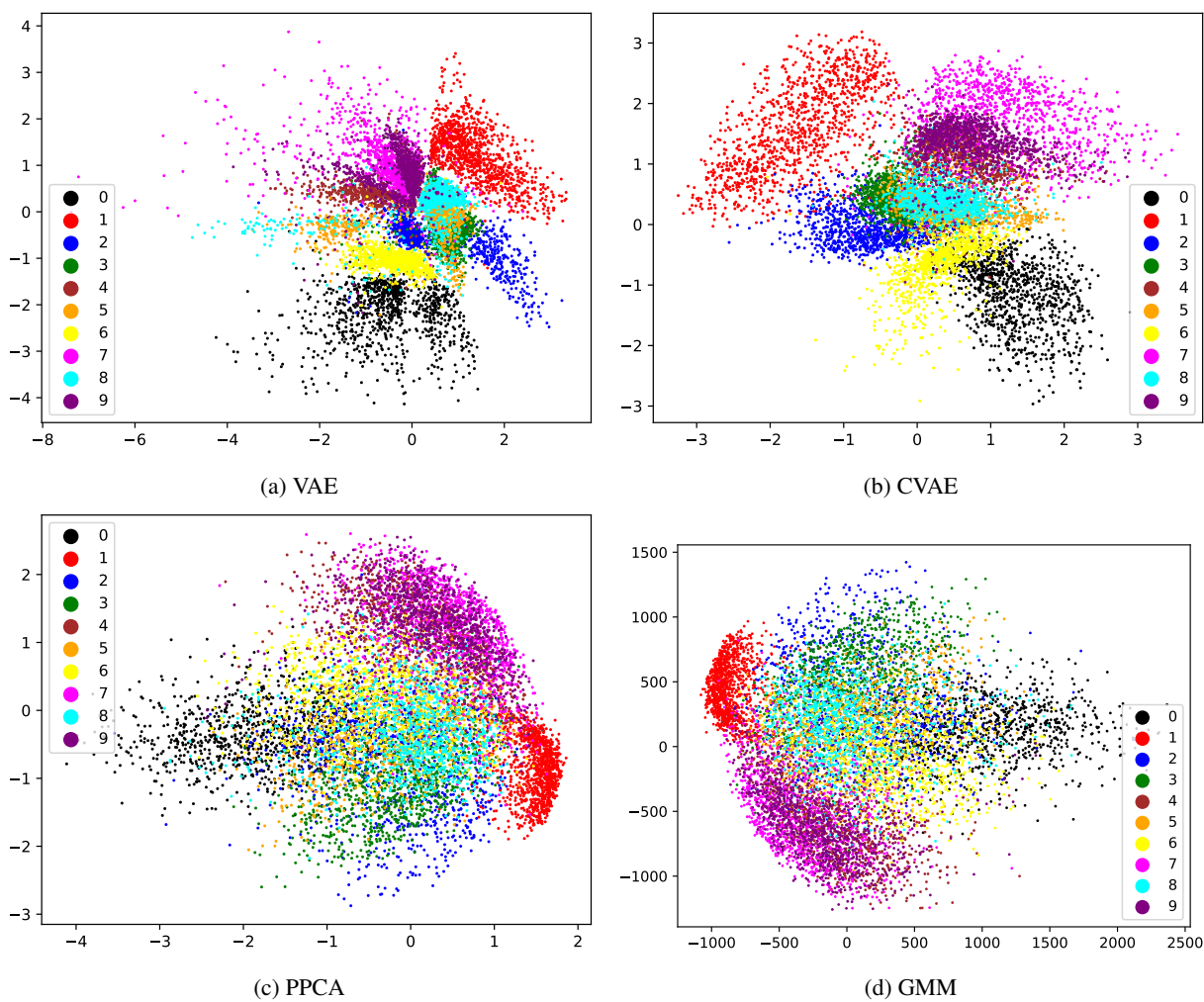


Figure 3: Clustering on MNIST test (projection to latent space) using trained density models.

2 Function fitting

2.1 Fitting a GP with Pyro

2.2 Bayesian Optimization

3 Bibliography

Christopher M Bishop and Nasser M Nasrabadi. *Pattern recognition and machine learning*, volume 4. Springer, 2006.

Appendices

A Extra figures

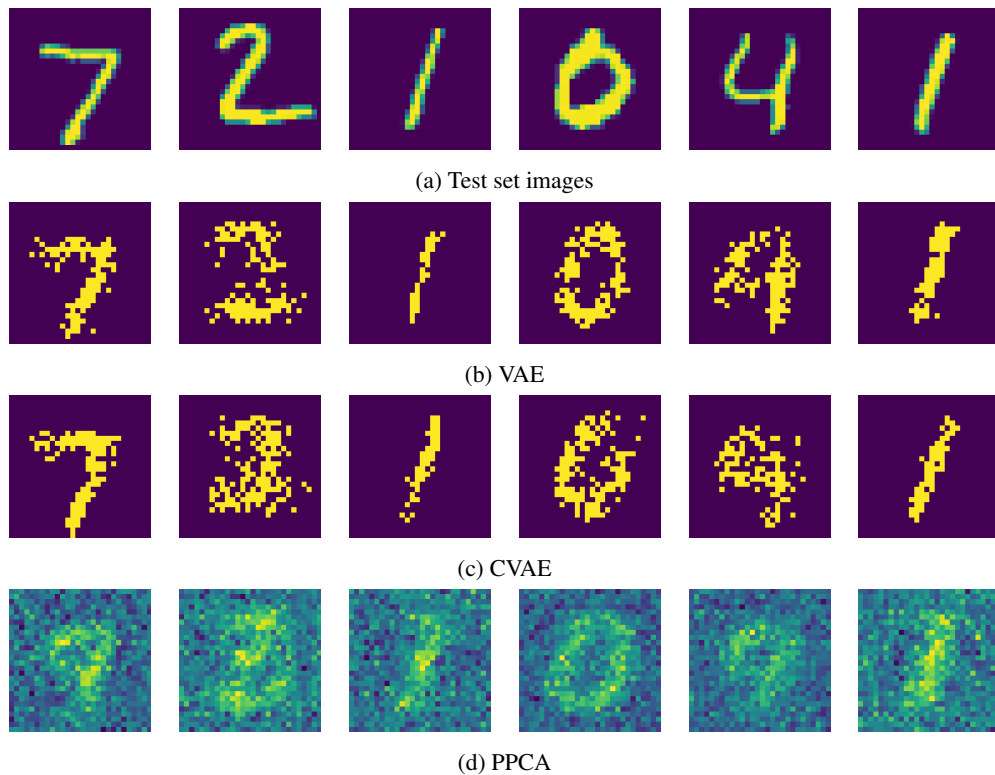


Figure 4: Comparison of MNIST test set images and corresponding reconstructions sampled from density models